J. Fluid Mech. (1980), *vol.* 100, *part* 4, *pp.* 673–689
Printed in Great Britain

Flow past a thin, inflated lenticular aerofoil

By B. G. NEWMAN AND M.-C. TSE
Department of Mechanical Engineering, McGill University, Montreal, Canada

(Received 10 July 1979 and in revised form 11 December 1979)

A study has been made of the flow past thin, inflated lenticular aerofoils at zero angle of incidence. The configuration is an idealization of the flow past long low inflated buildings when the effects of the earth's boundary layer are neglected. It is shown theoretically, and confirmed experimentally, that the non-dimensional tension coefficient in the inflated membranes comprising the aerofoil is a unique function of the internal pressure coefficient divided by the square root of the excess-length ratio. This applies for excess length ratios up to at least 0·05 which corresponds to a thickness-to-chord ratio, wind off, of 0·28. The aerofoil is found to become unstable at negative internal pressures corresponding to tension coefficients of approximately 0·4.

The theory has also been used to predict the shape of the aerofoil and the pressure distribution over it. With increasing wind speed at positive internal pressures, the membrane theoretically changes shape from a circular arc to a form involving inflexion points and in all cases the contours are symmetrical about the half-chord point. The non-dimensional membrane slope at the leading and trailing edges agrees fairly well with the experimental values. However, the measured pressure distributions show some fore-and-aft asymmetry and the maximum thickness is slightly downwind of the half-chord point. Nevertheless the comparison between theory and experiment is satisfactory for small values of the excess-length ratio.

1. Introduction

The present paper is concerned with low speed flow about thin symmetrical lenticular aerofoils at zero incidence. The aerofoils are formed by inflating a flexible impervious membrane which is anchored at both leading and trailing edges. The effect of varying both the pressure inside the aerofoil and the length of the membrane is considered. Wind-tunnel measurements of pressure distribution and membrane tension have been made for internal pressure coefficients ranging from $-0{\cdot}12$ to $+3{\cdot}22$, and for ratios of membrane length to chord ranging from 1·006 to 1·052. These results are compared with an analysis based on inviscid theory for thin aerofoils. The assumption of thinness leads to two useful simplifications. First the boundary condition giving the local pressure difference across the membrane may be stated directly in terms of the rate of change of slope of the surface. Secondly the shape of the aerofoil may be established by sources and sinks whose strengths depend only on the local slope of the surface. This leads to a solution and an interesting collapse of independent parameters, which is similar to that for single-membrane aerofoils, or sails, of small camber at low incidence (Thwaites 1961; Nielsen 1963).

The present work was suggested by the need to predict the tension in the skin of

0022-1120/80/4526-1910 $02.00

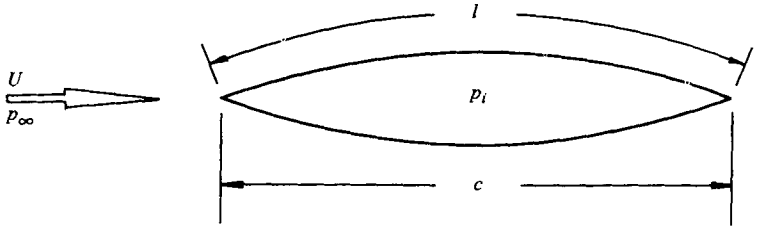

FIGURE 1. Inflated lenticular aerofoil at zero incidence.

long pneumatic structures which are sometimes used as, for example, storage buildings, greenhouses or to cover sports arenas (Herzog 1976). They often consist of a single inflated membrane inflated to a pressure which is determined by the anticipated wind speed. In the past *ad hoc* wind-tunnel tests have been made of models of particular shape such as spherical radomes (Kamrass 1954) and buildings which are hemispheres, or semicylinders with quarter-spherical ends (Niemann 1970). However, no general theory exists for predicting the membrane tensions in a wind even for simple geometries.

2. Theory

2.1. *Preliminary considerations*

Consider two-dimensional incompressible flow past a lenticular inflated aerofoil at zero angle of incidence (see figure 1). The aerofoil is symmetrical with a chord c and a total membrane length of $2l$; the internal pressure is p_i.

If the membrane does not oscillate, dimensional analysis indicates that there are three criteria of similarity for the above situation and these may be chosen as

$$C_{p_i} = \frac{p_i - p_\infty}{\frac{1}{2}\rho U^2}, \quad \frac{l}{c} \quad \text{and} \quad Re = \frac{\rho U c}{\mu},$$

where μ is the coefficient of viscosity and ρ is the air density.

With wind off ($U = 0$), the shape of each side of the aerofoil is a circular arc of radius $R = T/(p_i - p_\infty)$, where T is the membrane tension per unit span (see figure 2).

From figure 2

$$l = 2R\theta \quad \text{and} \quad c = 2R\sin\theta = 2R(\theta - \tfrac{1}{6}\theta^3 + \ldots).$$

Eliminating θ from these equations for small θ, or excess-length ratio $(l-c)/c$, gives

$$\frac{c}{R} = \frac{c(p_i - p_\infty)}{T} = \sqrt{(24)}\left(\frac{l-c}{c}\right)^{\frac{1}{2}} = \frac{8h_0}{c}, \tag{1}$$

where h_0 is the half-thickness of the aerofoil.

With wind on the overall tension increases and there is also a small change of tension ΔT from leading edge to trailing edge due to the skin friction. This is given approximately by $\Delta T \simeq C_f \frac{1}{2}\rho U^2 l$, where C_f is the skin-friction coefficient. Comparing this with the static value (1),

$$\frac{\Delta T}{T} = \frac{C_f}{C_{p_i}}\sqrt{24}\,\frac{l}{c}\left(\frac{l-c}{c}\right)^{\frac{1}{2}} = 8\frac{C_f}{C_{p_i}}\frac{l}{c}\frac{h_0}{c}. \tag{2}$$

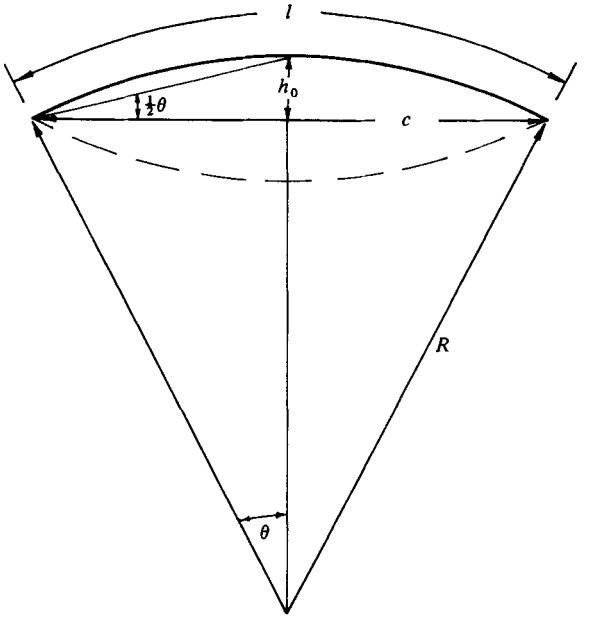

FIGURE 2. Geometry with the wind off.

The typical order of magnitude of C_{p_i} is 1 and C_f should not exceed 0·005. Hence, $\Delta T/T \simeq 0{\cdot}04h_0/c$ for small $(l-c)/c$. Thus the change of tension is usually unimportant if h_0/c is less than about $\frac{1}{4}$. Under wind load, therefore, it is reasonable to assume that T is constant and thus the non-dimensional tension coefficient

$$C_T = \frac{T}{\frac{1}{2}\rho U^2 c} = f\left(C_{p_i}, \frac{l-c}{c}, Re\right). \tag{3}$$

It is anticipated that, at high Re, scale effects will be relatively unimportant.

2.2. *Analysis for a thin aerofoil*

Assuming inviscid flow, the aerofoil shape is established by distributing sources of strength m per unit length along the x axis. Thus, the source strength over length dx_1 at x_1 is $m\,dx_1$ (see figure 3). Since the aerofoil is thin, the velocity *within* the aerofoil may be taken as U for the purpose of obtaining the first approximation for m (Thwaites 1960). Applying continuity for the small control volume $2y_1\,dx_1$,

$$m\,dx_1 = 2U\frac{dy_1}{dx_1}dx_1.$$

At x, the velocity associated with the source $m\,dx_1$ is

$$du = -\frac{m\,dx_1}{2\pi(x_1-x)}.$$

Thus, the total velocity at x is

$$u = U - \int_0^c \frac{2U\frac{dy_1}{dx_1}dx_1}{2\pi(x_1-x)}. \tag{4}$$

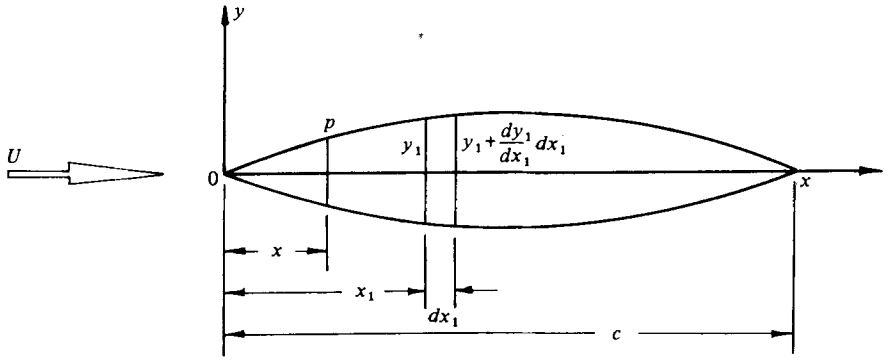

FIGURE 3. Notation for thin aerofoil theory.

The associated pressure p at x given by Bernoulli's equation

$$p_\infty - p = \tfrac{1}{2}\rho(u^2 - U^2) = \rho U(u - U) \quad \text{for } u - U \text{ small.} \tag{5}$$

For local equilibrium of the membrane

$$p_i - p = \frac{T}{R} = -T\frac{d^2y}{dx^2} \tag{6}$$

since the aerofoil is thin. Combining (4), (5) and (6),

$$-\frac{C_T c}{2}\frac{d^2y}{dx^2} = \frac{C_{p_i}}{2} - \frac{1}{\pi}\int_0^c \frac{\frac{dy_1}{dx_1}dx_1}{(x_1 - x)}, \tag{7}$$

where

$$C_T = \frac{T}{\frac{1}{2}\rho U^2 c} \quad \text{and} \quad C_{p_i} = \frac{p_i - p_\infty}{\frac{1}{2}\rho U^2}.$$

The length l of each half of the membrane

$$l = \int_0^c \left[1 + \left(\frac{dy}{dx}\right)^2\right]^{\frac{1}{2}} dx = \int_0^c \left[1 + \frac{1}{2}\left(\frac{dy}{dx}\right)^2\right] dx. \tag{8}$$

Putting $z = y/C_{p_i}c$ and $z_1 = y_1/C_{p_i}c$ and replacing x/c by x, equations (7) and (8) become

$$-\frac{C_T}{2}\frac{d^2z}{dx^2} = \tfrac{1}{2} - \frac{1}{\pi}\int_0^1 \frac{\frac{dz_1}{dx_1}dx_1}{x_1 - x}, \tag{9}$$

$$\frac{1}{C_{p_i}^2}\frac{l-c}{c} = \frac{1}{2}\int_0^1 \left(\frac{dz}{dx}\right)^2 dx. \tag{10}$$

Equation (9) establishes that z is a function of C_T. Thus from (10)

$$C_T = f\left[C_{p_i}\left(\frac{l-c}{c}\right)^{-\frac{1}{2}}\right]. \tag{11}$$

Thus, in the context of thin aerofoil theory, the individual independent parameters of equation (3), viz. C_{p_i} and l/c, form a combined parameter $C^* = C_{p_i}((l-c)/c)^{-\frac{1}{2}}$.

A similar combination of parameters arises in the analysis of a two-dimensional sail

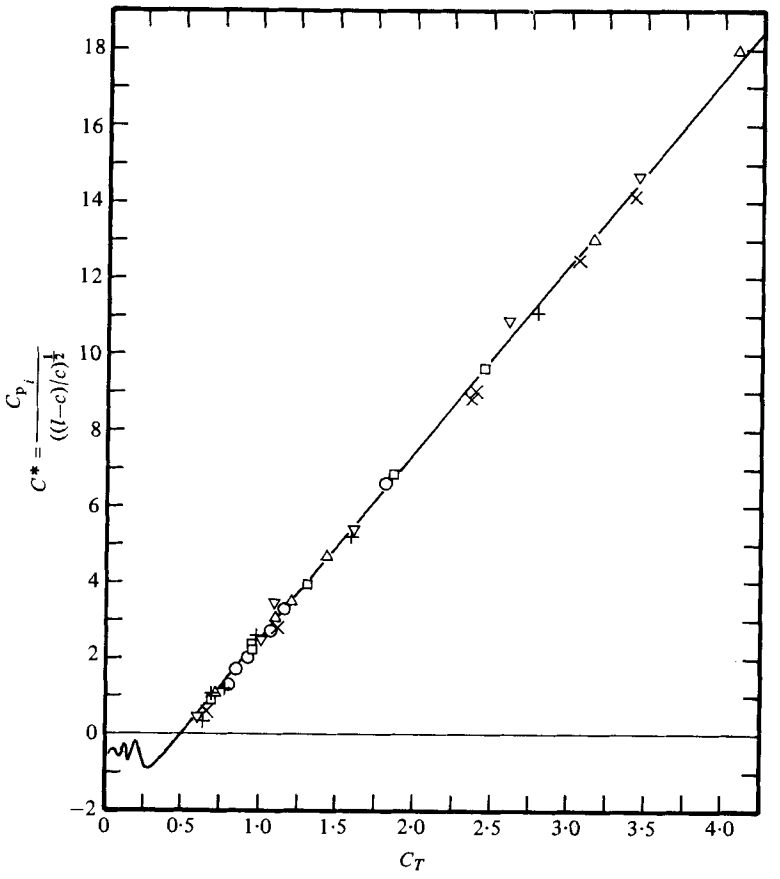

FIGURE 4. Comparison between theory and experiment for C_T when $C_{p_i} > 0$. The points are experimental and the line is theoretical. Reynolds number between $2{\cdot}9 \times 10^5$ and $9{\cdot}8 \times 10^5$.

	h/c	$(l-c)/c$
△	0·046–0·057	0·0056–0·0082
▽	0·051–0·067	0·0078–0·0122
□	0·070–0·077	0·0140–0·0171
○	0·093–0·099	0·0228–0·0256
+	0·100–0·107	0·0267–0·0312
×	0·135–0·140	0·0480–0·0518

by thin aerofoil theory for camber and incidence (Thwaites 1961; Nielsen 1963). In this case

$$C_T = f\left[\alpha\left(\frac{l-c}{c}\right)^{-\frac{1}{2}}\right],$$

where α is the angle of incidence of the sail and is analogous to C_{p_i} for the lenticular aerofoil.

The numerical solution of equation (9) is conventional in terms of a Fourier series for z. Substituting $x = \frac{1}{2}(1-\cos\theta)$, $x_1 = \frac{1}{2}(1-\cos\theta_1)$ and

$$z = \sum_{n=1}^{n=\infty} A_n \sin n\theta.$$

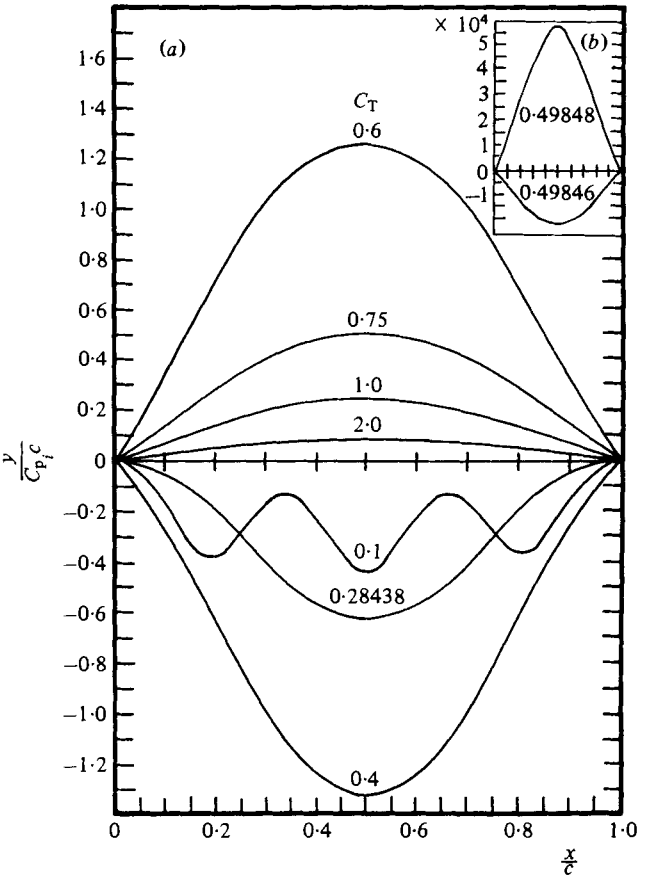

FIGURE 5. Theoretical membrane shapes for various C_T.

This expression correctly gives $z = 0$ at $x = 0$ and 1.

Equation (9) becomes

$$2C_T \sum_n \frac{nA_n}{\sin^3\theta}(n\sin\theta\sin n\theta + \cos\theta\cos n\theta) = \tfrac{1}{2} + \frac{2}{\pi}\sum_n nA_n \frac{\pi\sin n\theta}{\sin\theta}$$

or
$$C_T \sum_n nA_n[(n+1)\cos(n-1)\theta - (n-1)\cos(n+1)\theta]$$
$$= \tfrac{1}{8}(3\sin\theta - \sin 3\theta) + \sum_n nA_n[\sin n\theta - \tfrac{1}{2}(\sin(n+2)\theta + \sin(n-2)\theta]. \quad (12)$$

It might be anticipated that the aerofoil will have fore-and-aft symmetry so that values of A_n for n even are zero. This result can be proved formally from equation (12) by replacing θ by $\pi - \theta$ and subtracting the resulting equation from (12).

The pressure distribution over the membrane is given by equations (4) and (5),

$$C_p = \frac{p - p_\infty}{\frac{1}{2}\rho U^2} = 2\left(1 - \frac{u}{U}\right) = -4C_{p_i}\sum_n A_n \frac{\sin n\theta}{\sin\theta}. \quad (13)$$

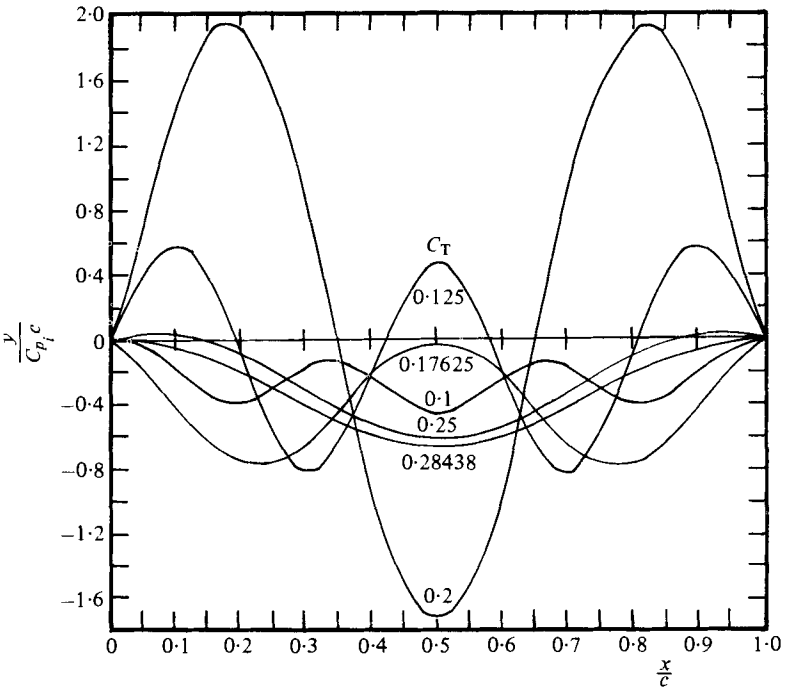

FIGURE 6. Theoretical membrane shapes for various C_T and negative C_{pi}.

The non-dimensional length of the membrane is, from equation (10),

$$\frac{1}{C_{p_i}^2}\left(\frac{l-c}{c}\right) = \frac{1}{C_T^2}\int_0^\pi \left[\tfrac{1}{4}\cos\theta + \sum_n A_n \cos n\theta\right]^2 \sin\theta\, d\theta,$$

using the integrated form of (9). Thus,

$$\frac{1}{C_{p_i}^2}\left(\frac{l-c}{c}\right) = \frac{1}{2C_T^2}\sum_n\sum_m A_n A_m\left[\frac{1}{m+n+1} - \frac{1}{m+n-1} + \frac{1}{m-n+1} - \frac{1}{m-n-1}\right], \quad (14)$$

in which A_1 is replaced by $\frac{1}{4} + A_1$.

The slope $(dy/dx)_0$ at $x = 0$ or 1 is found by integrating equation (9) from $\theta = 0$ to $\frac{1}{2}\pi$,

$$\frac{(dy/dx)_0}{C_{p_i}} = \left(\frac{dz}{dx}\right)_0 = \frac{1}{C_T}\left[\tfrac{1}{2} + 2\sum_n A_n\right]. \quad (15)$$

The coefficients A_n are determined by solving equation (12) numerically. Since n is odd, it is sufficient to use equal increments of θ between 0 and $\frac{1}{2}\pi$, the number of increments being equal to the chosen number of terms A_n. Trials were made using from 10 to 25 terms. They showed that $C_{p_i}(c/(l-c))^{\frac{1}{2}}$ derived from equation (14) using 15 terms was within 0·1 % of the value using 25 terms for all values of C_T except very close to the values for zero C_{p_i}, viz. $C_T = 0{\cdot}4985$. All the results presented here are for 20 terms.

The universal curve (equations (11) and (14)) relating C_T to $C^* = C_{p_i}(c/(l-c))^{\frac{1}{2}}$ is shown in figure 4. It is found that $C^* = 0$ for $C_T = 0{\cdot}49847$ and that the curve for positive C^* is very nearly a straight line of slope $\sqrt{24}$; C^*/C_T asymptotically approaches the wind-off value $\sqrt{24}$ for very large values of C_T. For $C_T < 0{\cdot}49847$, C^* is negative,

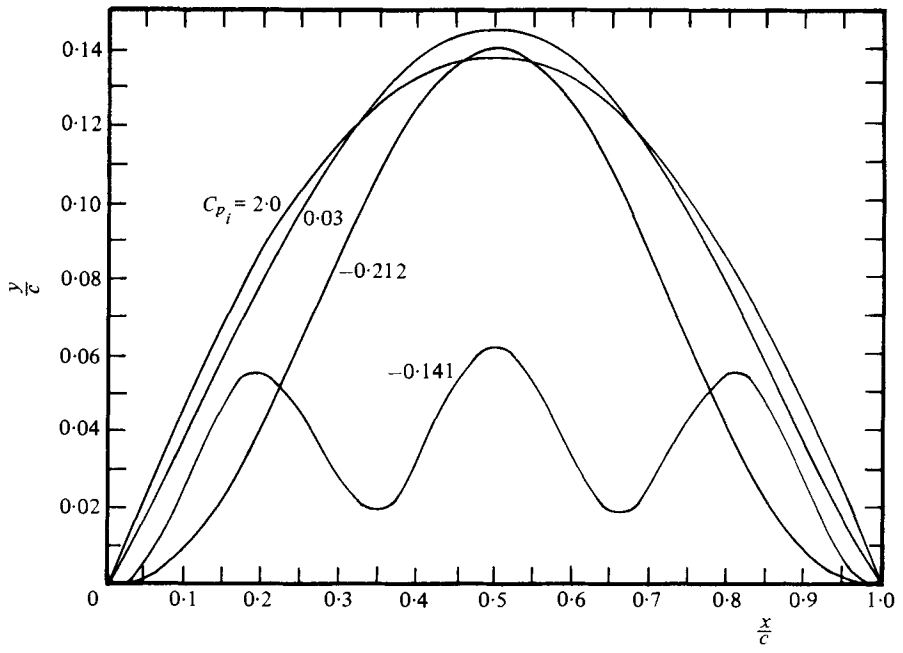

FIGURE 7. Theoretical membrane co-ordinates for a fixed membrane length, $(l-c)/c = 0{\cdot}05$.

which implies that the pressure inside the membrane is below that of the free stream. There can then be several values of C_T for a particular C^*. The corresponding membrane shapes are shown in figures 5 and 6, where the ordinate y/c has been divided by C_{p_i} in accordance with the theory. Thus as C^* tends to zero the apparent length of the membrane increases to large values. The curves for C_T near 0·49847 have therefore been separately plotted in figure 5(*b*). In figure 5 the shape for $C_T = 2$ is close to a circular arc, which is equivalent to a parabola in thin aerofoil theory. As C_T is reduced the shape becomes straighter near the leading and trailing edges. For C_T less than about 0·6 inflexion points appear where the external pressure is locally equal to that inside the membrane. The shapes shown in figure 6 are exclusively for $C^* < 0$, and several are wavy. In practice it may be impossible to obtain a wavy shape which is both stable and steady, and indeed those shapes which cross the x/c axis ($C_T = 0{\cdot}125$ and 0·20) are obviously unrealistic.

In order to eliminate the apparent change of membrane length with C^* or C_T the results for a particular $(l-c)/c = 0{\cdot}05$ have been plotted in figure 7 using as ordinate y/c rather than y/cC_{p_i}. The results now show physically how the membrane changes shape as C_{p_i} is altered. As the internal pressure is reduced the height of the membrane increases slightly and then at negative pressures develops inflexion points and finally becomes wavy.

The present theory is based on the assumption that the aerofoil is thin. Some idea of the maximum permissible thickness for this approximation is obtained by comparing the calculated pressure distribution for symmetrical and rigid circular arcs with the corresponding exact solution. The latter is obtained from a Kármán–Trefftz

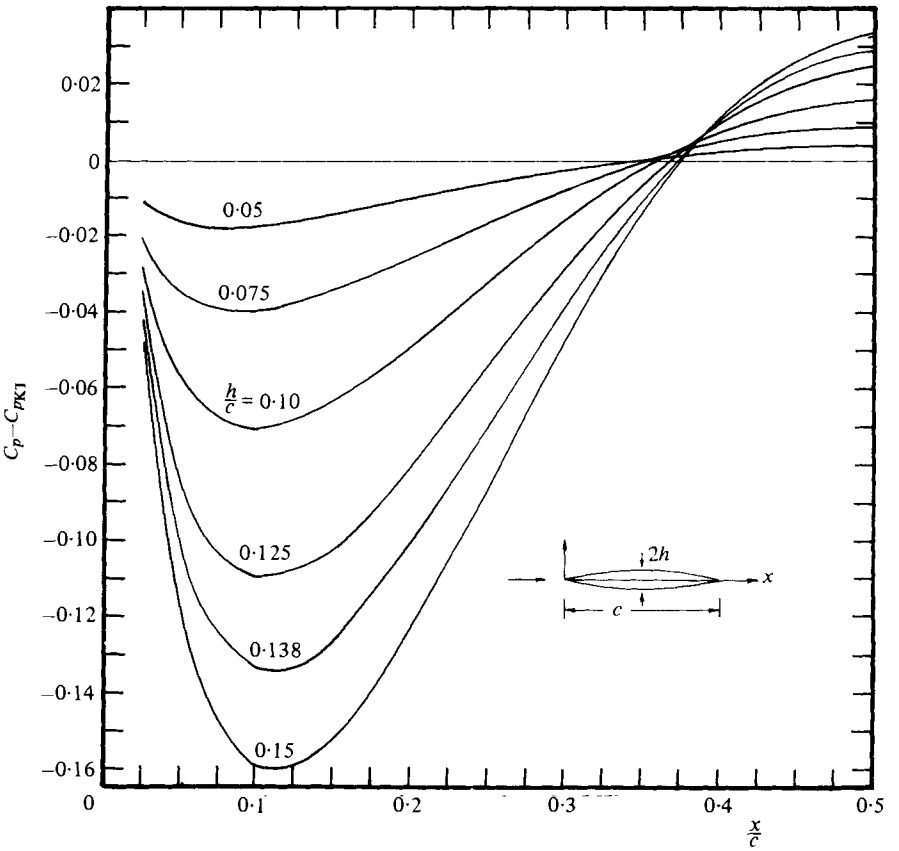

FIGURE 8. Comparison of the pressure distribution for a circular-arc lenticular aerofoil. C_p is from thin aerofoil theory. C_{pKT} is from a Kármán–Trefftz transformation.

conformal transformation of flow about a circle and is given by Milne Thomson (1958). It is found that the maximum discrepancy between the two theories occurs at $x/c = 0·10$ and that the pressure coefficients differ there by about 0·07 when $h/c = 0·10$. The error at mid-chord is however less than 0·02 for the same height-to-width ratio. The complete comparison for various values of h/c is shown in figure 8.

3. Experiment

3.1. *Description of the apparatus*

Measurements were made on a lenticular aerofoil mounted vertically in the 760 × 430 mm blower wind tunnel in the McGill Aerodynamics Laboratory (Wygnanski & Gartshore 1963). This tunnel has a maximum speed of 40 m s^{-1} and the pressure in the working section is close to atmospheric pressure. The inflated aerofoil consisted of an impervious sleeve supported by thin steel wedges at the leading and trailing edges. The chord of the aerofoil could be adjusted slightly between 371 and 382 mm. The wedges contained an angle of 11° and protruded 61 mm through the floor and ceiling of the tunnel, where they were mounted on flexures for force measurement.

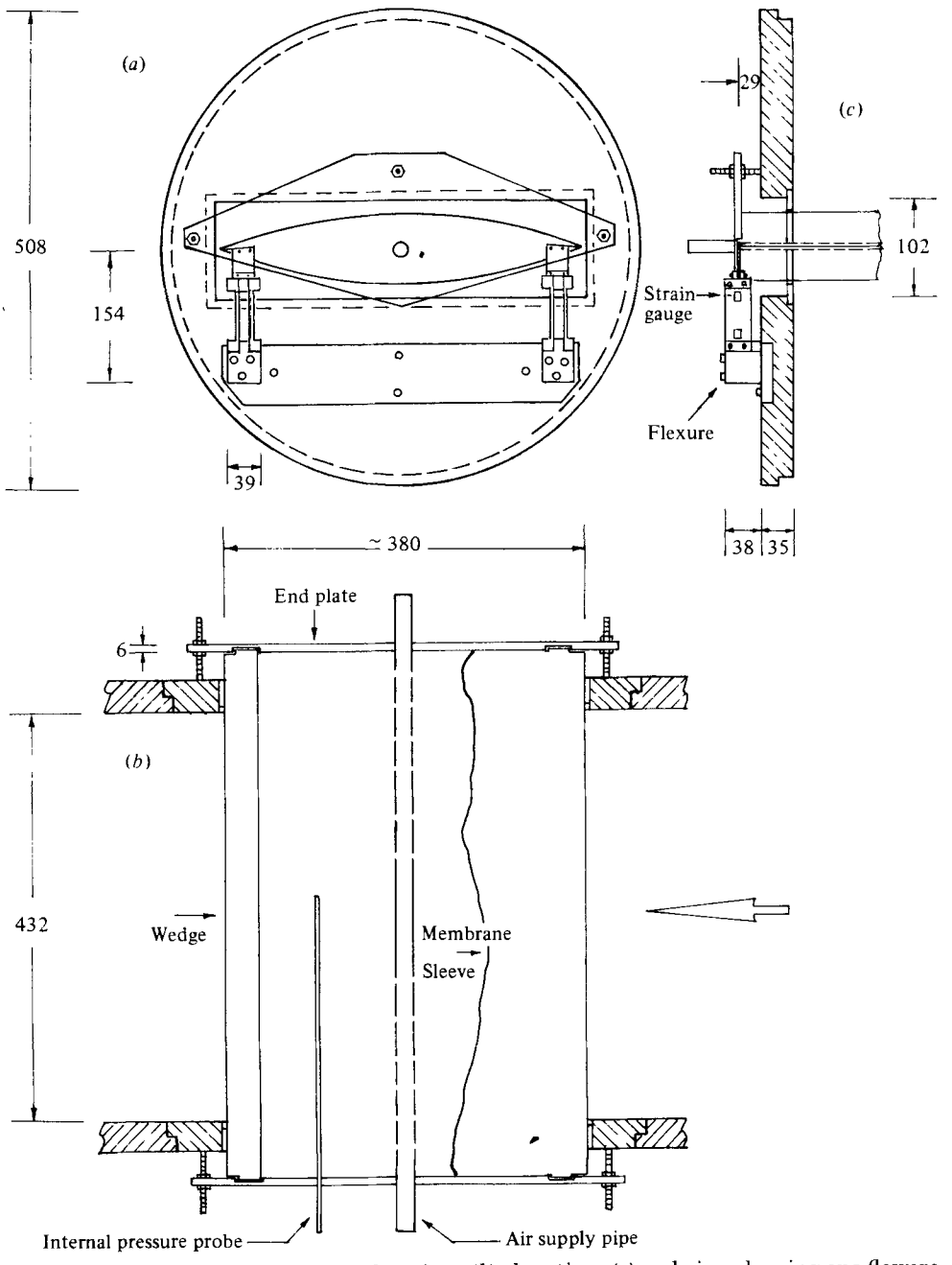

FIGURE 9. Details of the apparatus: (*a*) plan view; (*b*) elevation; (*c*) end view showing one flexure. Dimensions are in millimetres.

These flexures were instrumented with resistance strain gauges and arranged so as to measure the force in the direction of the aerofoil chord. The sleeves (three in all) were made of flexible, impervious, rip-stop nylon, 25 g m^{-2}, a light closely-woven cloth which is used for spinnaker sails on small boats. In each case, the cloth was sewn to form a uniform sleeve and the seam was placed at the trailing edge of the model.

The inflated sleeve was passed through suitably shaped holes cut out of Plexiglas sheets which were mounted in the floor and ceiling of the wind tunnel. The size and shape of these holes was altered to suit the particular sleeve under test. The ends of the sleeve rested on Plexiglas end plates mounted outside the tunnel and outboard of the flexures. The leakage there was made as small as possible and was replenished by continually supplying air to the inside of the model. In this way, the spanwise tension in the sleeve was negligibly small and the two-dimensional boundary condition for the membrane (equation (6)) was valid. A sketch of the experiment is shown in figure 9.

Apart from the fore-and-aft force on the leading and trailing edge wedges, the following additional measurements were made:

(i) The pressure inside the model was measured by means of open-ended tubes and static tubes. These gave essentially the same reading of pressure, thereby substantiating that the air movement within the model was sufficiently small to be unimportant.

(ii) The local pressure outside the model was measured using a static tube placed close to, and locally aligned with, the surface of the membrane. To do this, the static tube was mounted on a rotatable traversing gear attached to one wall of the tunnel.

(iii) The inclinations of the membrane at the leading and trailing edges were measured using the measured alignment of the static tubes at these positions. The membrane tension could then be derived directly from the fore-and-aft force on the supporting wedges.

(iv) The maximum thickness of the inflated membrane with wind off was measured using calipers.

3.2. *Experimental procedure*

The chord line of the wedges was aligned with the wind stream by first testing the arrangement without a membrane. A pressure tap was located in the leading edge of the forward wedge and the overall angle of attack was adjusted until this tap measured the total pressure in the tunnel. The aerofoil was then effectively at zero incidence.

Three membrane sleeves were tested which, when combined with the allowable adjustment in chord length c, gave values of $(l-c)/c$ ranging from 0·006 to 0·052.

For each arrangement initial measurements were made with the *wind off*. The values of maximum thickness and chord enabled the radius of curvature of the circular membranes and the membrane angles at leading and trailing edge to be calculated. The values of curvature multiplied by the internal gauge pressure, $p_i - p_\infty$, then gave a value for the tension in the membrane which could be compared with the values calculated from the wedge forces and the membrane angles. When the ends of the membrane were adjusted to minimize the leakage there, these values typically agreed within 1 %.

Since the membrane stretched slightly under load its length l with wind on had to be determined from the wind-off measurements. The procedure was as follows. First the loads on the ends of the membrane which protruded outside the tunnel were determined by assuming that wind-off conditions applied there. These loads were then subtracted from the measured forces on each wedge to give the force associated with the air flow alone. When combined with the membrane angles this gave the tension in the membrane with wind on. The value of l was assumed to be identical with the

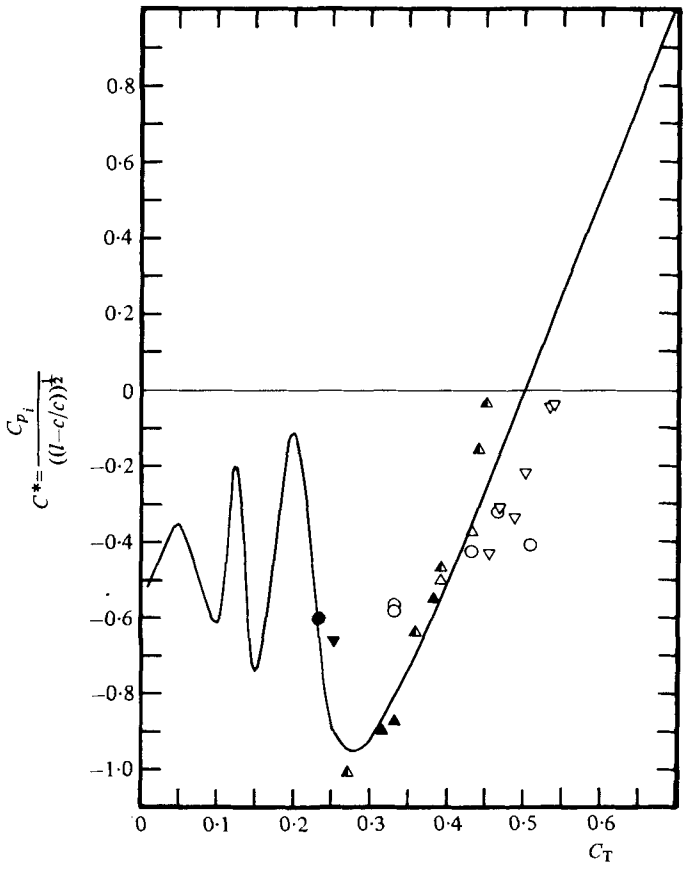

FIGURE 10. Comparison between theory and experiment for C_T when $C_{p_i} < 0$. The points are experimental and the line is theoretical. Reynolds number between $3{\cdot}3 \times 10^5$ and $9{\cdot}8 \times 10^5$. The ranges of $(l-c)/c$ are: △, 0·0106–0·0170; ▽, 0·0277–0·0328; ○, 0·0350–0·0380. Half-filled symbols denote partial collapse; totally filled symbols denote total collapse.

calculated value under the same tension with wind off. The two values of the tension obtained from the forces on the two wedges usually agreed within 1 % and the average value was recorded.

Wind tunnel corrections to wind speed were applied for both solid and wake blockage (Pankhurst & Holder 1952). The drag coefficient for wake blockage was taken to be equal to that of the corresponding N.A.C.A. 00xx aerofoil with the same thickness-to-chord ratio. The corrections to speed amounted to + 1 % for $h/c = 0{\cdot}05$ and + 3 % for $h/c = 0{\cdot}14$. These corrections have been applied to C_T and C_{p_i}, but not to the local pressure coefficient C_p.

Tests were made for values of C_{p_i} between $-0{\cdot}12$ to $+3{\cdot}22$ and Reynolds numbers based on chord from $2{\cdot}9 \times 10^5$ to $9{\cdot}8 \times 10^5$.

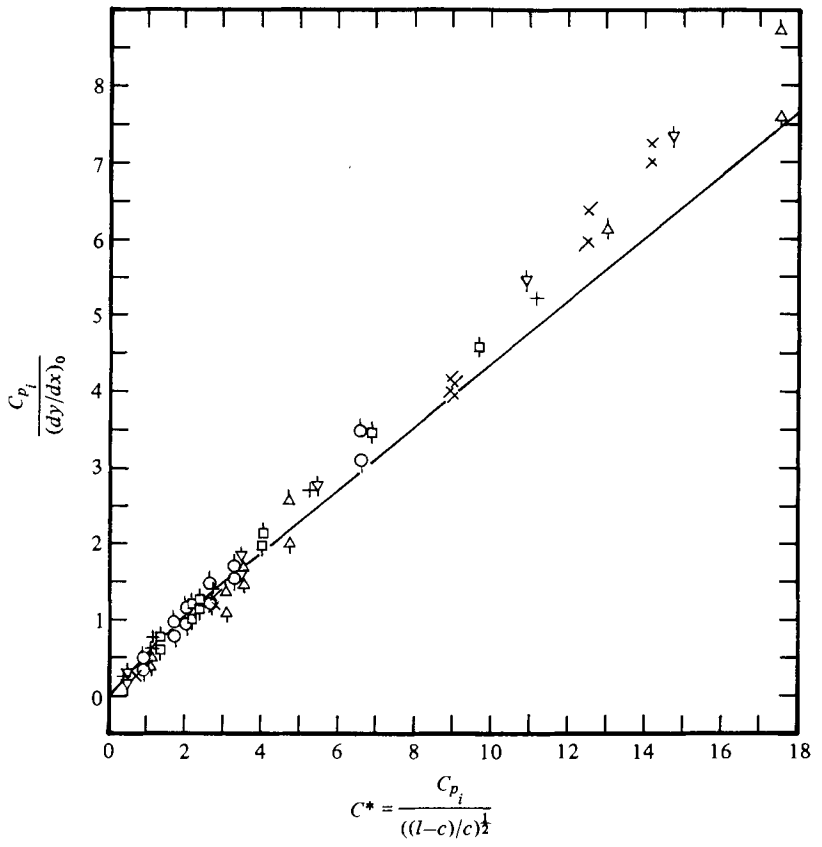

FIGURE 11. Comparison between theory and experiment for the normalized membrane slopes. Flags on the experimental points: ○, leading edge; ○, trailing edge. The legend is the same as figure 4.

4. Discussion of results

Initially visual tests were made to detect separation on the aerofoil as the length and thickness of the sleeve were changed. To do this very light tufts were attached to the surface. For positive values of C_{p_i} and $(l-c)/c > 0{\cdot}02$ it was found that there were small regions of separation (typically $< 0{\cdot}05c$ wide) over the rear half of the aerofoil near the floor and ceiling of the tunnel. However no separation could be seen at mid-span even for the largest value of $(l-c)/c$ which was tested, namely $(l-c)/c = 0{\cdot}052$ corresponding to $h_0/c = 0{\cdot}14$.

For large values of C_{p_i} the shape of the membrane on either side was apparently circular. As the internal pressure was reduced the shape of the membrane appeared to alter qualitatively in the manner predicted by the theory (figures 5 and 7). In particular the thickness increased slightly and the shape tended to become concave near the leading and trailing edges. It was found that the membrane was stable even for slightly negative values of C_{p_i}. However as the internal pressure was reduced the membrane began to oscillate and then progressively collapse near the leading edge. At still lower pressures the forward part of the membrane collapsed completely.

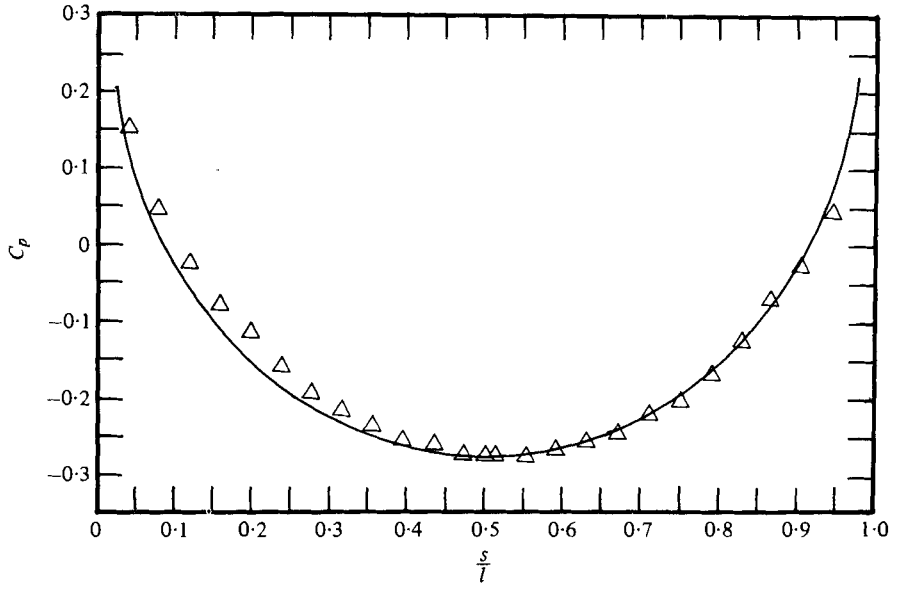

FIGURE 12. Experimental pressure distribution compared with theory – thin case. $C_T = 4{\cdot}08$; $C_{p_t} = 1{\cdot}54$; $(l-c)/c = 0{\cdot}0077$; $Re = 3{\cdot}1 \times 10^5$.

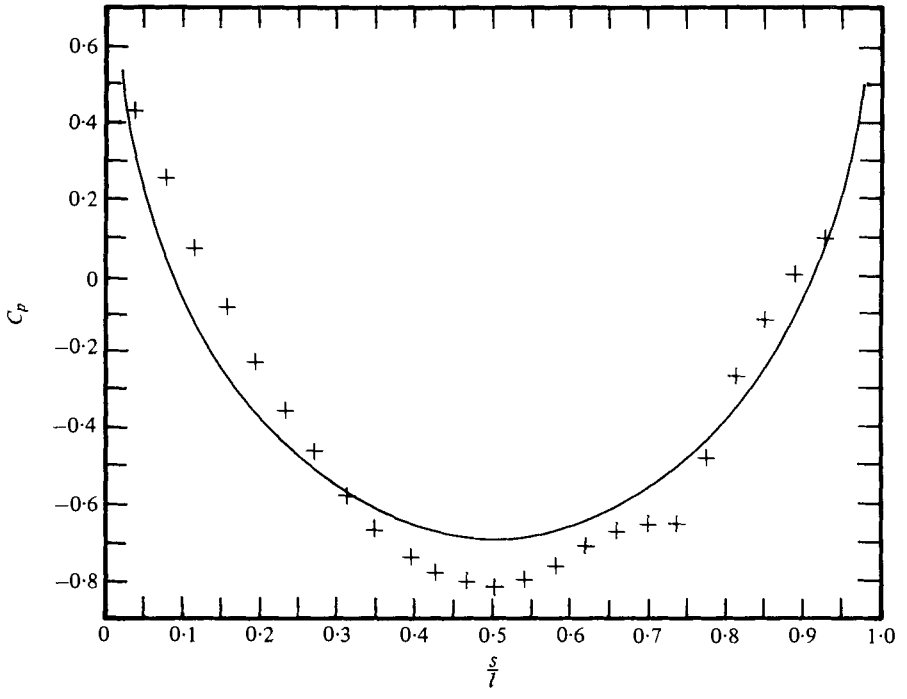

FIGURE 13. Experimental pressure distribution compared with theory – thick case. $C_T = 2{\cdot}38$; $C_{p_t} = 2{\cdot}02$; $(l-c)/c = 0{\cdot}0516$; $Re = 3{\cdot}4 \times 10^5$.

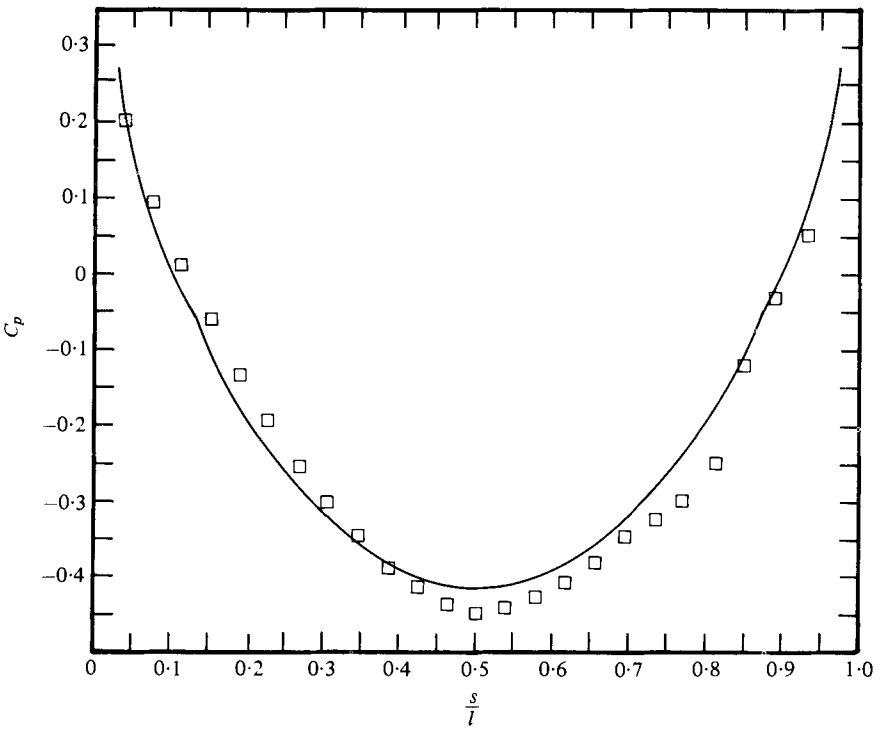

FIGURE 14. Experimental pressure distribution compared with theory – low C_T.
$C_T = 0{\cdot}952$; $C_{p_t} = 0{\cdot}284$; $(l-c)/c = 0{\cdot}014$; $Re = 5{\cdot}3 \times 10^5$.

Partial or total collapse typically occurred for values of C^* corresponding to C_T less than 0·4, although the exact value seems to be somewhat lower for large values of $(l-c)/c$. The theory (figure 6) predicts a wavy membrane for values of C_T less than about 0·28 and such a steady shape was never observed experimentally. Thus membrane collapse begins for values of C_T somewhere between 0·3 and 0·4, with higher values for small h/c.

The experimental measurements of the tension coefficient C_T are plotted against the reduced pressure coefficient C^* in figure 4 and compared with the theoretical prediction. The agreement is very good. Some results for negative C^* are compared with the theory in figure 10. These are less accurate because the portion of the membrane outside the tunnel was usually collapsed and the end corrections were therefore uncertain. For some of the results the membrane exposed to the wind was also either partially or fully collapsed and these are identified on the figure. Nevertheless agreement with the theory is still surprisingly good. The leading and trailing edge slopes as calculated from equation (15) are compared with the measurements of these quantities in figure 11. For low values of C^* it is seen that the trailing-edge angles are generally larger than the leading-edge angles and both are shown on the figure. This difference is attributed to the increase in boundary-layer thickness as the air flows over the aerofoil which has the effect of decreasing the pressure towards the rear and hence the curvature of the membrane there. Thus the maximum thickness is moved rearwards slightly until a new equilibrium is established. In general the agreement between theory and

experiment in figure 11 is not as good as in figure 4 and this can probably be attributed to difficulty in measuring the edge angles when these angles are small.

The measured pressure distributions are compared with the predictions for three cases in figures 12, 13 and 14. The results are plotted against s/l, the non-dimensional distance measured along the surface of the membrane. With a flexible surface it was easier to identify positions using this parameter rather than the conventional chordwise distance x/c. For large values of C_T the membranes are nearly circular and for small values of $(l-c)/c$ the agreement between theory and experiment is good. As $(l-c)/c$ is increased boundary-layer effects become increasingly important and in figure 13 there is even evidence of a separation bubble at $s/l = 0{\cdot}70$. The agreement between theory and experiment is now less satisfactory. For small values of C_T and $(l-c)/c$ the agreement also deteriorates somewhat over the rear of the aerofoil as can be seen in figure 14. The disagreement over the front of the aerofoil in figures 13 and 14 can be attributed mainly to the use of thin aerofoil theory (see figure 8).

It is of interest to consider to what extent the present theory predicts the tension in a long low inflated structure when the wind is blowing at right angles to the building. The inflated lenticular aerofoil is a reflexion plane model for this case, but only if boundary-layer effects are neglected. In practice the building is within the relatively thick boundary layer of the earth and the flow therefore separates and reattaches both at the front and back of the structure. However these separation bubbles may be relatively insignificant if the height of the building is small. Thus the customary discrepancy between tests in uniform flow in simulated boundary layers, which are particularly important for three-dimensional buildings (Simiu & Scanlan 1978) may be much smaller in this case. Indeed recently we have made tests (Goland 1980) on a two-dimensional inflated building with a height-to-width ratio of 0·18 which was immersed in an artificially thickened boundary layer about 20 times as thick as the height of the building. Even though the height ratio of the building was somewhat larger than the maximum ratio investigated on the lenticular aerofoil, the present theory predicted the membrane tension fairly well, underestimating it by about 10 %. The wind velocity at the height corresponding to the top of the building was chosen as the reference value for this comparison.

It is therefore concluded that the present theory for lenticular aerofoils may be useful in providing a preliminary estimate for the membrane tension in a long, low, inflatable building when the wind is blowing at right angles to it.

REFERENCES

GOLAND, D. 1980 Two-dimensional inflated buildings in a cross wind. M.Eng. thesis. McGill University.

HERZOG, T. 1976 *Pneumatic Structures*. Oxford University Press.

KAMRASS, M. 1954 Wind-tunnel tests on a 1/24th scale model air-supported radome and tower. *Cornell Aero. Lab. Rep.* UB-909-D-1.

MILNE THOMSON, L. N. 1958 *Theoretical Aerodynamics*, 3rd. MacMillan.

NIELSEN, J. N. 1963 Theory of flexible aerodynamic surfaces. *Trans. A.S.M.E.* E, *J. Appl. Mech.* **30**, 435–442.

NIEMANN, H. J. 1972 Wind tunnel experiments on aeroelastic models of air-supported structures. *Proc. Int. Symp. on Pneumatic Structures, Delft*, paper 5–11.

PANKHURST, R. C. & HOLDER, D. W. 1952 *Wind-Tunnel Technique*. London: Pitman.

SIMIU, E. & SCANLAN, R. H. 1978 *Wind Effects on Structures.* Wiley.

THWAITES, B. 1960 *Incompressible Aerodynamics.* Oxford University Press.

THWAITES, B. 1961 The aerodynamic theory of sails. I. Two-dimensional sails. *Proc. Roy. Soc.* A **261**, 402–422.

WYGNANSKI, I. & GARTSHORE, I. S. 1963 General description and calibration of the McGill 17 in. × 30 in. blower cascade wind tunnel. *McGill Univ. Mech. Engng Res. Lab. Tech. Note* 63–7.